Materials & Design 261 (2026) 115357

Contents lists available at ScienceDirect

Materials & Design

journal homepage: www.elsevier.com/locate/matdes

Influence of oxygen plasma on the material properties of Two-Photon polymerized microstructures

Jone M. Elorrieta [a], George Mathew [b], Clara Garcia-Sacristan [c], Jorge A.L. Solaiman [c], Livia Martegiani [c], Ricardo García [c], Eider Berganza [b,c,*]

[a] Centro de Investigaciones Energéticas, Medioambientales y Tecnológicas (CIEMAT), Av. Complutense 40, 28040 Madrid, Spain
[b] Institute of Nanotechnology (INT), Karlsruhe Institute of Technology (KIT), Kaiserstraße 12, 76131 Karlsruhe, Germany
[c] Instituto de Ciencia de Materiales de Madrid (ICMM-CSIC), Sor Juana Inés de la Cruz 3, 28049 Madrid, Spain

ARTICLE INFO

Keywords:
Two-photon polymerization
3D printing
Post-processing
Young's modulus
Mechanical properties
Raman spectroscopy
Bimodal AFM

ABSTRACT

O_2 plasma exposure is a convenient postprocessing method for refining 3D microstructures fabricated by two-photon polymerization, which provides an effective way to achieve sub-micrometer resolution with remarkable feature control. Unlike pyrolysis, which despite being a widespread methodology to decrease feature size, it alters the properties of the bulk material, O_2 plasma etching primarily modifies the surface. In this work, we explore the influence of plasma etching treatments on the material properties of 3D microstructures. We examine the resulting modifications to key parameters relevant to various applications: surface roughness, mechanical properties, and material composition. Our findings reveal a two-stage effect: low exposure times reduce surface roughness, while prolonged exposure leads to an increase in roughness. Nanomechanical properties are strongly affected, with the Young's modulus of the surface increasing by an order of magnitude, indicating a stiffening effect. Raman spectroscopy evidences that the observed stiffening is not due to the formation of a carbonized layer but rather due to further crosslinking. These results highlight the need to carefully evaluate the impact of O_2 plasma etching on the final properties of 2PP microstructures when designing fabrication processes to ensure the necessary physical and chemical properties for the desired application.

1. Introduction

In the last years, two-photon polymerization (2PP) has gained significant attention, revolutionizing 3D printing of microstructures with its high precision and ability to build intricate shapes. Being at the forefront of 3D printing technologies with sub-micrometer printing capabilities, the use of 2PP has been extended to different fields, ranging from optics, [1] biomedical engineering, [2] metamaterials, [3] to micro robotics [4].

The development of femtosecond lasers enabled the realization of this technology, by facilitating a confined polymerization reaction due to its high photon density, within a photosensitive material. By scanning the laser focal point along the photoresist, arbitrary three-dimensional objects can be fabricated. Despite the versatility and potential of the technique, the 2PP community still aims to develop smaller features, seeking strategies to target the smallest achievable voxel sizes. [5] The resolution of 2PP is primarily restricted by the diffraction limit of the focusing optics, as well as the photoinitiator concentration, laser power stability, and material properties, which affect polymerization precision and ultimately determine the feature size [6,7].

In this regard, various approaches have been explored to overcome its resolution limitations, based either on (i) modifying the optics of the setup,[8–12] (ii) adding free radical quenchers to the photoresist [5,13–15] or (iii) following post-processing methods (Fig. 1).[16] The application of stimulated emission depletion (STED) to 3D laser lithography yielded freestanding features with cross sections of around 100 nm,[9,10] while more recent advances, which include its combination with chemical quenchers,[15] have further pushed the resolution limits, achieving feature sizes down to 50 nm.[11,15] Despite this achievement, the combination of 2PP and STED requires a setup upgrade requiring complex optics and alignment. A more straightforward alternative lies in using a laser with a smaller wavelength, which is also not always possible to implement in commercially purchased setups. [12] Post-processing approaches are conducted for multiple purposes, offering considerable advantages in terms of simplicity. [17–20] Aiming at reducing the dimensions to beat the resolution given by the voxel size,

* Corresponding author.
E-mail address: eider.berganza@csic.es (E. Berganza).

https://doi.org/10.1016/j.matdes.2025.115357
Received 28 May 2025; Received in revised form 1 December 2025; Accepted 15 December 2025
Available online 18 December 2025

pyrolysis[21–25] and O_2 plasma treatments[16,26–28] have been proposed.

Pyrolysis treatments yield isotropic shrinkage of microstructure volume, as subjecting the polymeric structures to a heat treatment in absence of O_2 causes thermal decomposition with subsequent loss of mass and shrinkage. [22–29] This process leads to material transformation, converting organic materials into carbonized structures, which is interesting for MEMS or applications requiring either conductive or mechanically robust structures. [23] Pyrolysis treatments, however, can be challenging when applied to complex geometries, often complicating the process, as the properties of the pyrolyzed material are highly dependent on the temperature and duration of the treatment. This leads to variability in the properties of the final structure and can yield the appearance of internal stresses and deformations, cracking or asymmetric shrinkage due to the adhesion to the substrate [24].

Alternatively, exposure to O_2 plasma for dry etching constitutes an easily accessible approach readily adopted by the increasing number of researchers working with 2PP. In contrast to pyrolysis, it produces an isotropic etching of the exposed microstructure surfaces, enabling the fabrication of extremely fine features. [26] On the other hand, highly intricate and high aspect ratio structures can be produced, by incorporating sacrificial support features that can be removed using plasma in a later step treatment, which avoids distortions during development. [27] O_2 plasma is also used to get rid of entire 3D printed polymeric structures that serve as molds in subsequent lithographic steps that yield a metallic structure, such as electroplating, [29,30] or physical vapor deposition coating [31].

As O_2 plasma is widely used in nano and microfabrication processes to achieve desired material properties – removal of organic contaminants, surface activation or promoting hydrophilicity –, it is well known to affect physical and compositional properties of the material surface. [32] During exposure of polymers to O_2 plasma, highly reactive species, such as O_2 ions, radicals and excited molecules react with its surface, breaking down the polymer chains and forming volatile products.

While the physical and chemical changes occurring as a result of pyrolysis on structures grown via 2PP has been reported [22], no study, to the best of our knowledge, has investigated the influence of O_2 plasma exposure, despite been highly relevant to avoid compromising the properties or functionalities of the intended applications.

In this context, the work here presented thoroughly assesses the extent of O_2 plasma-induced changes, focusing on the nanomechanical properties, roughness, compositional modifications and wettability using various complementary characterization techniques. The results underscore the necessity of considering these effects during fabrication process design.

2. Materials and methods

2.1. Materials

Pentaerythritol triacrylate (PETA) was purchased from Santa Cruz Biotechnology, Inc., Germany, and the photoinitiator Phenylbis (2,4,6-trimethylbenzoyl) phosphine oxide (Irgacure 819) was obtained from Sigma-Aldrich, USA. The photoresist was prepared by dissolving 20 mg of Irgacure 819 in 980 mg of PETA. The mixture was sonicated for 120 min at 60 °C to ensure complete dissolution of the photoinitiator powder.

2.2. Two-photon polymerization

Microfabrication Process: Microstructures were fabricated using a commercial two-photon polymerization (2PP) system (PPGT2, Nanoscribe GmbH, Germany). A 780 nm femtosecond pulsed laser and a 63×/1.4 plan-apochromat objective (Zeiss, Germany) were employed for laser exposure. The power was fixed at 15 mW and writing speed 3000 μm/s. Borosilicate coverslips were secured and scanned with laser

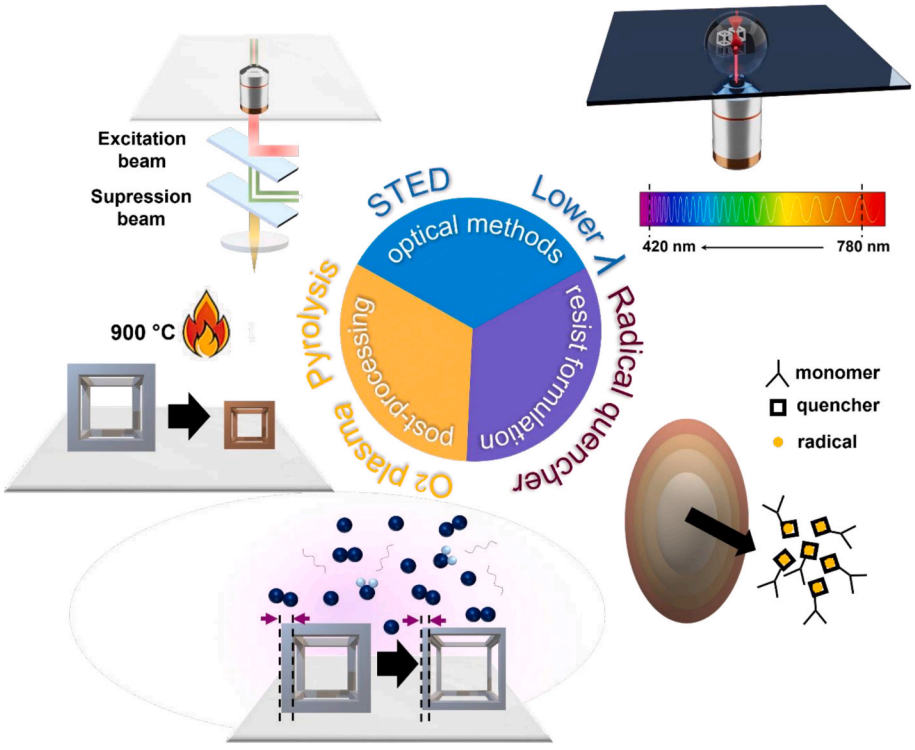

Fig. 1. Different methods used to lower the resolution of 2PP printed microstructures. Methods based on modifying the setup to minimize the voxel size comprise the combination of STED with direct laser writing and the reduction of the femtosecond laser wavelength. Post-processing methods are based on pyrolysis at 900 °C to carbonize the sample to let it shrink isotropically, and etching through O_2 plasma to ablate the exposed surfaces. Adding free-radical quenchers to the photoresist formulation allows confining the effect on radical diffusion.

radiation, controlled by galvanometric mirrors. After polymerization, samples were cleaned in isopropanol for 24 h and dried with nitrogen.

Design and Parameters: Structural designs were created in Blender and imported into Describe (Nanoscribe GmbH, Germany). For nanomechanical characterization and spectroscopy experiments, 40x40x5 μm^3 cubic structures were designed with a 0.1 μm hatching and slicing distance to minimize surface roughness. For the calibration of the plasma etching, 50x2x2 μm^3 lines were patterned on the substrate.

2.3. O_2 plasma treatment

The samples were exposed to O_2 plasma in two systems from Diener Electronics ATTO system (Germany), with an available power of 200 W and an O_2 flux of 400 sccm. The power was kept at 100 W and the gas flux at 50 sccm unless otherwise stated.

The etching calibration was performed by repeatedly exposing the line patterns to O_2 plasma at different conditions and determining the changes in thickness via atomic force microscopy (AFM) after every step. AFM measurements were conducted with in tapping mode (amplitude modulation), using a scanning force microscope from Nanotec Electronica together with Nanosensors PPP-FMR probes. The obtained images were processed and analyzed using WSxM software.

2.4. Nanomechanical characterization

The Young's modulus maps were generated by bimodal AFM. A commercial AFM platform and software (Cypher S, Oxford Instruments, USA) was used in these experiments. The bimodal-AFM was operated in air in the amplitude modulation (first mode) and frequency modulation (second mode) configuration.[33] Mechanical excitation was used to excite the vibration of the cantilever. The experiments were performed with standard cantilevers (PPP-FM, NanoAndMore, Germany). Typical values of the resonant frequencies, force constants and quality factors in air were, $f_1 \sim 68$ kHz; $k_1 \sim 2.25$ N/m and $Q_1 \sim 185$, $f_2 \sim 437$ kHz; $k_2 \sim 92$ N/m and $Q_2 \sim 505$. Typical values of the free amplitudes A_0 and set-point A_{sp} amplitudes were, $A_{01} \sim 115$ nm, $A_{sp1} \sim (0.7–0.9)A_{01}$, $A_{02} \sim 0.5$ nm. The images were recorded at 2.44 Hz with 512x512 pixels.

2.5. Compositional characterization

Raman spectra were acquired by using a Horiba LabRAM HR Evolution spectrometer (Jobin Yvon Technology), at an excitation wavelength of 532 nm (50mW nominal laser power). The scattered radiation was collected in backscattering geometry through a 100x objective (Olympus BX41 microscope), dispersed using a 600 grooves/mm holographic grating, and recorded by a CCD detector (256x1024 pixels). The spectral resolution obtained in this configuration was better than 2 cm^{-1}. A typical spectrum was obtained in the 600 to 3400 cm^{-1} range, within 30–50 s of acquisition time and 2–3 accumulations. Spectra were recalibrated with the emission lines of a Ne lamp. The excitation laser power and acquisition times were optimized in order to prevent alteration of the samples.

2.6. Contact angle measurement

PETA was spin coated on glass substrates with 3000 rpm for 1 min and cured under a UV lamp of 405 nm wavelength for 10 min. After the plasma trearment, the WCA were measured using the sessile drop method with the OCA-20 system (DataPhysics Instruments GmbH, Germany).

2.7. Scanning Electron microscope imaging

The surface morphology of the samples was investigated using Scanning Electron Microscopy (SEM). Images were acquired on a Nova NanoSEM 230 microscope (FEI, Hillsboro, OR, USA). The imaging was performed under high vacuum conditions with an acceleration voltage of 2.5 kV and a consistent magnification of 12 000x.

3. Results and discussion

3.1. Etching behavior

O_2 plasma treatment is widely employed both to refine 2PP-fabricated microstructures or to remove printed features (see Supporting Information 1 for examples). To systematically evaluate its etching effects, we focus on the relationship between plasma processing parameters and their influence on Pentaerythritol triacrylate (PETA) structures. PETA, an acrylate-based monomer, is one of the most common resins utilized in 2PP. With this aim, straight lines were fabricated on a borosilicate substrate and their thickness was measured by AFM.

The samples were exposed to O_2 plasma with varying conditions (power and exposure time) and their thickness was measured after every step (see Supporting Information 2). Fig. 2 shows an etching behavior that can be adjusted to a parabolic curve. While low power (<20 W) provides accurate control and precise etching with tens of nanometers of accuracy, high power is more effective for the more rapid removal of material.

3.2. Induced surface roughness and evolution of nanomechanical properties

O_2 plasma can compromise surface properties of laser written structures, which critically impact needed features for good performance: specific stiffness for tissue engineering or soft microrobotics, minimal roughness for printed microlenses, etc. To assess the extent of such modifications during O_2 plasma treatment, solid cubes were fabricated, exposed to O_2 plasma for different times and their surface properties were inspected via bimodal AFM measurements (Fig. 3a).

This constitutes a well-established advanced nanomechanical characterization technique where two modes of oscillation of the cantilever are simultaneously excited.[33] It combines the sensitivity of the first resonance mode, used for topography, with a higher harmonic mode, that enhances the resolution for nanomechanical mapping of the sample. [34,35] Details about this measurement mode are given in Supporting Information 3. Young's modulus of the sample is given by analyzing the phase shift, amplitude and frequency changes resulting from tip-sample interactions. Topographic and Young's modulus images obtained on the surface of the printed solid cubes, exposed to O_2 plasma at increasing times, are shown in Fig. 3b.

Notice that the samples are printed with 100 nm slicing and hatching

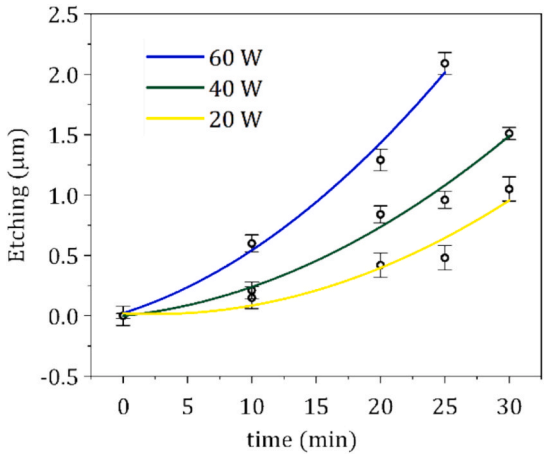

Fig. 2. Etched thickness of PETA by exposure to O_2 plasma, with different working powers and O_2 flux fixed at 100 sscm.

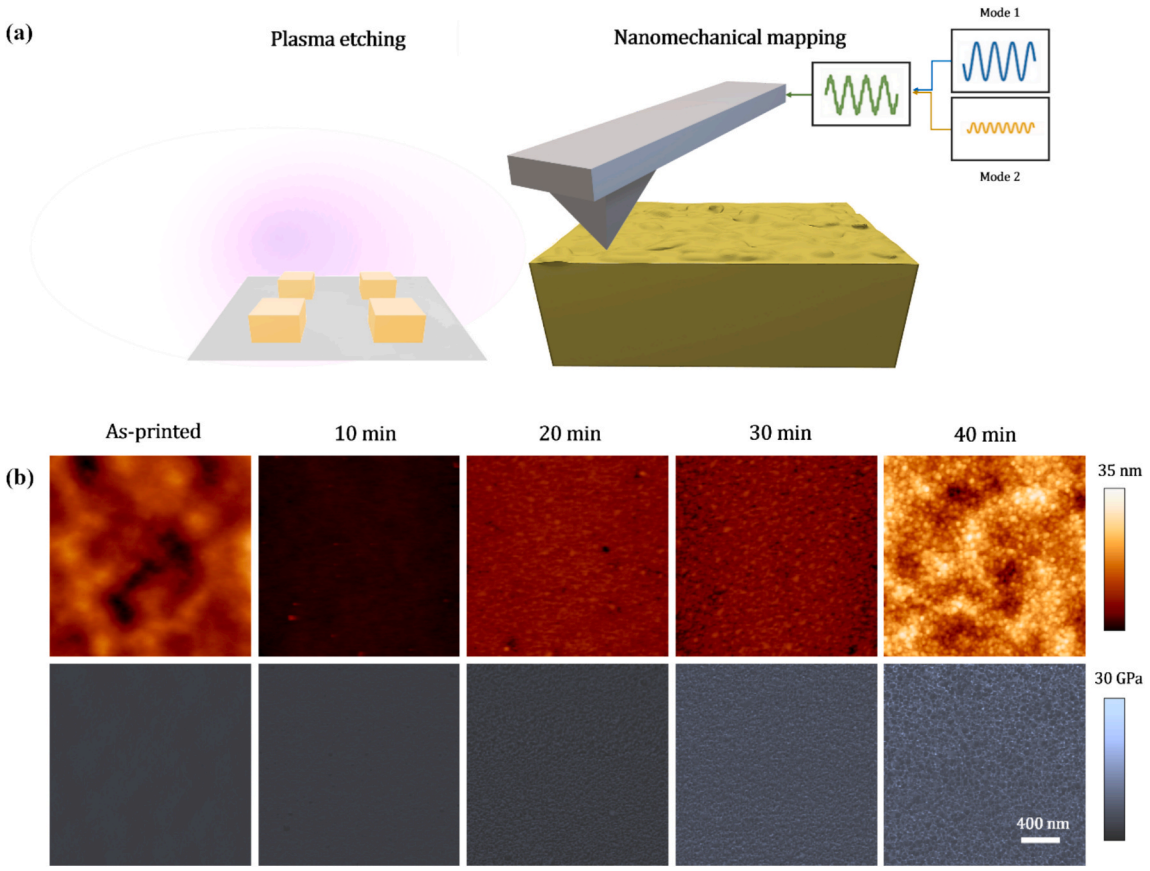

Fig. 3. Nanomechanical characterization. (a) Illustration of the followed steps for a nanomechanical characterization by bimodal AFM. (b) Obtained topographic (top) and Young's modulus (bottom) images for surfaces of microstructures grown by 2PP, exposed to O_2 plasma for increasing times.

parameters to minimize initial surface roughness, which leads to a moderate initial roughness of 10 nm (Fig. 3b). Subsequent topographic images show an increase in surface roughness at prolonged exposure times, with the exception of a flattening effect occurring at initial stages. Quantitative data, extracted with the software WSxM and shown in Figs. 4a and 4b, clearly reflect this result. The distribution of heights is gathered in a histogram, where the as-cast samples show a double-peak distribution with a wide dispersion of values. After 10 min of exposure to O_2 plasma, the roughness considerably decreases, as the peak shifts to lower values and displays the lowest dispersion. Surface roughness, quantified by Root Mean Square (RMS), is calculated for the images showing a Gaussian distribution of the topographic events and shows a non-linear increase with exposure time (Fig. 4b). As Fig. 4c illustrates, exposing the material to plasma stiffens the surface microstructure. Prolonged plasma etching increased the average Young's modulus from an initial 0.5 GPa to 4.2 GPa. This final stiffness is consistent with literature values for acrylate 2PP printed structures, acknowledging the typical variability associated with different writing parameters [36–38].

These results can be explained by several factors. Generally speaking, the O_2 plasma processes on polymeric materials boost –OH group formation, which can form hydrogen bonds with neighboring chains, increasing intermolecular interactions. The formation of –OH and other oxygen-containing groups can accompany etching, removing unsaturated bonds or oxidation, which can cause densification of the near-surface layer—polymer chains may become shorter, more oxidized, and form a denser, more glassy-like regions. All these reactions yield uneven material removal, causing surface roughness.

In 2PP printed polymers, the outcoming material constitutes a mixture of the intended polymer along with unreacted liquid monomer. During printing in the studied photoresist, PETA, the three acrylate groups (–CH=CH_2) undergo a chain reaction that creates covalent bonds between monomer units. Polymers are stronger materials than individual monomers because their long, repeating chains create a greater number of intermolecular forces.

The increase of local temperature in plasma exposure quite likely promotes heat induced crosslinking reactions, producing a harder material. The unreacted monomer is therefore more prone to be etched upon exposure to O_2 plasma, which gives rise to an anisotropic etching behavior.

However, shorter exposure times reduce the surface roughness down to 0.26-nm RMS, making this treatment an easily applicable solution to reduce unwanted nanoscale roughness inherent to 2PP. This might happen because during fabrication, the microstructure surface receives a smaller dose yielding higher content of unreacted monomer on the structure surface. For small hatching and slicing parameters, where the laser paths overlap, the inner parts of the structure are irradiated repeatedly, while the surface is irradiated only once. This makes the outer material more susceptible to O_2 plasma and yields a flattening of the surface until the less crosslinked layers are etched away. This effect is explained in detail in Supporting Information 4.

The increase in the surface's Young's modulus reported in Fig. 4c is also consistent with the selective etching of unreacted monomer. Nevertheless, Raman spectroscopy is used for complete chemical characterization to fully explain these physical changes.

Based on this outcome, we conclude that induced roughness and stiffness changes on the surface need to be evaluated when the microstructure fabrication process incorporates an O_2 plasma etching step.

3.3. Chemical modifications

Due to its power to reveal chemical changes, crosslinking density, and structural modifications, Raman spectroscopy has been extensively

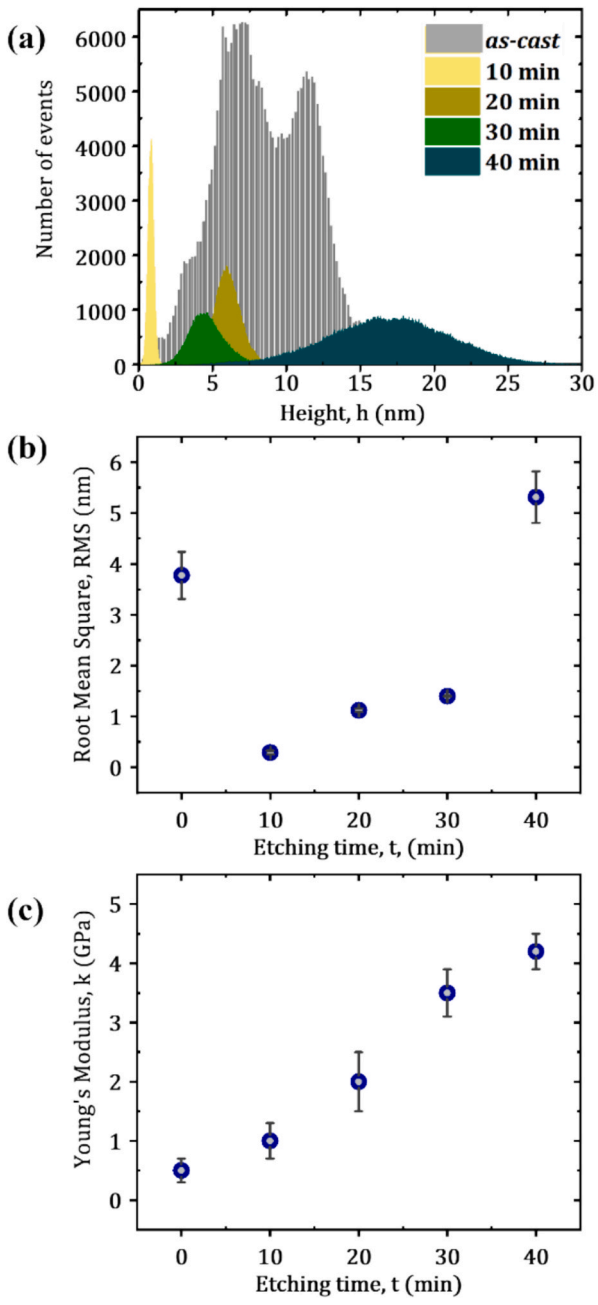

Fig. 4. Quantitative analysis. (a) Quantitative roughness analysis of the surface of the PETA solid cubes exposed to O_2 plasma. Evolution with exposure time of (b) surface roughness and (c) Young's modulus of the surface, extracted from nanomechanical maps with bimodal AFM.

used to study the polymerization kinetics during 2PP fabrication and shed light on the composition of microstructures grown by this technique. [39–42] These studies have evidenced the strong impact of the processing parameters, [43,44] the employed photoinitiator [45,46] or post-processing treatments [23] on the composition resulting from differences in the degree of consumption (DoC) within the material comprising the microstructures.

The DoC represents the fraction of monomers that have polymerized, directly influencing the mechanical and chemical properties of the fabricated structure. A higher DoC indicates increased crosslinking, leading to enhanced stiffness and stability, while an incomplete conversion may result in residual monomers affecting durability and biocompatibility. In acrylate-based photoresists, the DoC is estimated by examining the integrated intensities ratio of the bands corresponding to the C=C bond, located at ~ 1640 cm^{-1}, and the C=O bond, located at ~ 1730 cm^{-1}. Such ratio should decrease as a result of consumption of the monomer, *i.e.* as a result of polymerization. [22] Reference Raman spectra showing differences between the monomer and a typical as printed sample in the region of the mentioned peaks are included in Supporting Information 5. The DoC of the studied samples was calculated using the following expression, reported many times in the literature:

$$DoC = \left[1 - \left(\frac{A_{C=C}/A_{C=O}}{A'_{C=C}/A'_{C=O}}\right)\right] \text{ x } 100 \quad (1)$$

where $A_{C=C}$, $A_{C=O}$, $Á_{C=C}$ and $Á_{C=O}$ represent the integrated intensities of the corresponding C=C and C=O Raman bands in the 2PP structures and the non-polymerized resin, respectively.

Nanomechanical characterization indicates that the surface of the polymeric microstructures changes composition after extended exposure to O_2 plasma. It is reasonable to think that this stiffening is caused by superficial material carbonization. To assess whether a carbon layer is formed on the surface, solid cubes were printed and heated to 450 °C to induce carbonization. The Raman spectrum of this carbonized sample, which serves as reference sample, was compared to that of an as printed microstructure (Fig. S43a). The spectrum shows the intense characteristic D and G Raman bands associated with disordered and graphitic carbon structures [47].

The D band, appearing at around 1350 cm^{-1}, is linked to disorder-induced vibrations in sp^2 carbon systems and originates from the breathing modes of aromatic rings, requiring structural disorder to be Raman-active. The G band, found near 1580 cm^{-1}, corresponds to the in-plane stretching vibrations of sp^2 carbon atoms in graphitic structures and is characteristic of well-ordered graphitic domains. The intensity ratio of the D and G bands, I_D/I_G, used to estimate the degree of disorder and graphitization in carbonized materials, [48] shows a high degree of disorder as a consequence of the heating treatment. In this sense, if the samples exposed to O_2 plasma presented a superficial carbon layer, we would detect it in the corresponding Raman spectra, by identification of at least a minor contribution in the D-G bands region.

Therefore, Raman measurements were conducted on the samples subjected to increasing O_2 plasma exposure times, whose nanomechanical characterization had suggested a change in their surface composition (Figs. 3 and 4). Results in Fig. 5 show the most relevant cases (higher RMS values, Fig. 4b) and indicate the absence of graphitic or disordered carbon after 10 and 40 min of O_2 plasma exposure, as no trace of the D or G peaks are detected in the 1300–1600 cm^{-1} region.

However, a slight but unequivocal decrease of the signal-to-noise ratio is appreciated in the case of the longest exposed microstructure (40 min), which could be ascribed to the increase of the sample surface roughness (see Fig. 4b) and consequent dispersion of the light. In addition, a very subtle decrease of the C=O peak relative intensity for this same sample might be indicative of small changes in the DoC, as a result of increased polymer to monomer ratio during plasma exposure.

Raman spectroscopy measurements typically cover a depth of few micrometers, thus averaging over the sample volume in these microstructures. While a thin carbon layer on the surface should still be observable due to the inherently strong intensity of its corresponding peaks, [49] small changes in other bonding features of the superficial structure, such as the integrated intensities ratio of the C=C and C=O peaks for the different samples, can be challenging to detect. Based on the characterization results, we propose that local changes to the material's surface—such as the selective etching of unreacted monomers or the formation of strong covalent bonds via dehydration reactions of hydroxyl groups—significantly stiffen the material surface, excluding the formation of a carbon layer during the process.

Given the observed signs of a probable subtle change in the DoC for a long plasma exposure time, we considered the effect of temperature. Prolonged O_2 plasma treatments induce heating of the chamber and

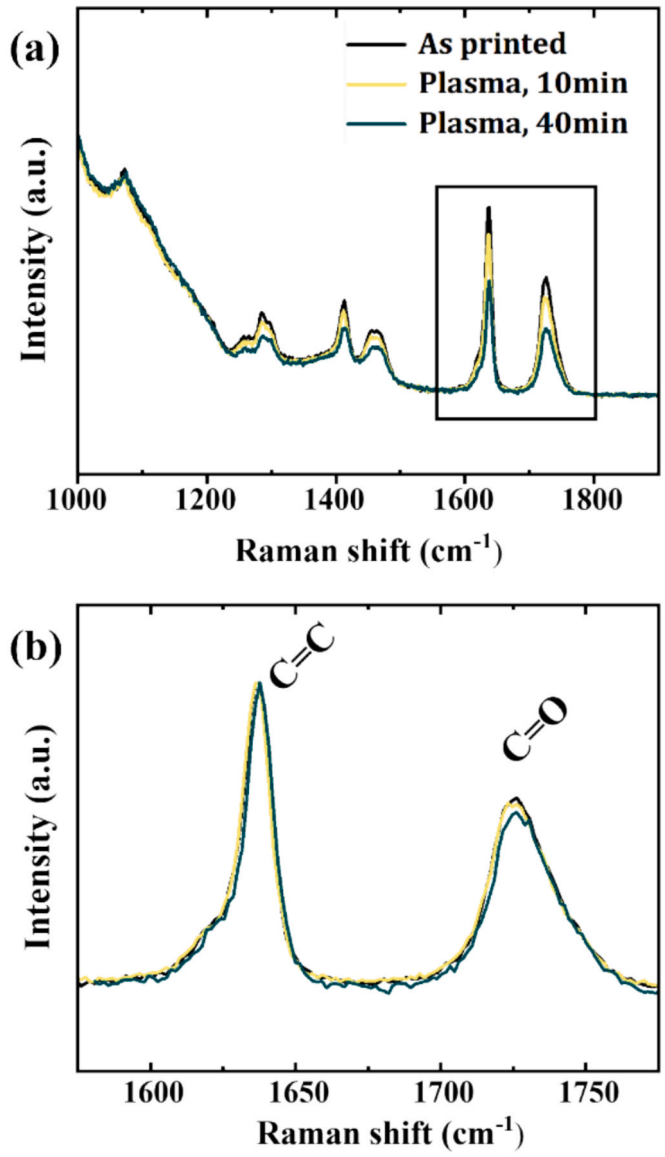

Fig. 5. Raman spectra in microstructures exposed to O_2 plasma for different times. (a) Comparison of the Raman spectrum of an as printed microstructure with those of two subjected to O_2 plasma for 10 and 40 min, respectively. (b) Zoom on the C=C and C=O peaks region for the three spectra of (a), normalized in such zone.

exposed sample. In order to assess the effect of temperature, an in-depth characterization of samples exposed to 20 min plasma treatments under controlled temperature (35, 50 and 60 °C) was conducted, and the results compared to those regarding an as printed microstructure and a sample solely subjected to temperature (heated on hot-plate for 20 min at 60 °C).

To control the temperature, the chamber was pre-heated at the desired temperatures before the samples were introduced in the chamber and irradiated for *intermediate* times, with the aim of maintaining a constant temperature during the treatment, while causing a measurable effect. Fig. 6a shows the Raman spectra acquired on the as printed reference, the temperature-subjected sample, and the temperature-controlled plasma exposed samples.

All the treated samples present the same overall features as the as printed microstructure, confirming that also in those cases no superficial carbonization was produced. With the aim of better addressing the differences in the DoC, the five Raman spectra were normalized in the region displaying the peaks corresponding to the C=C and C=O bonds

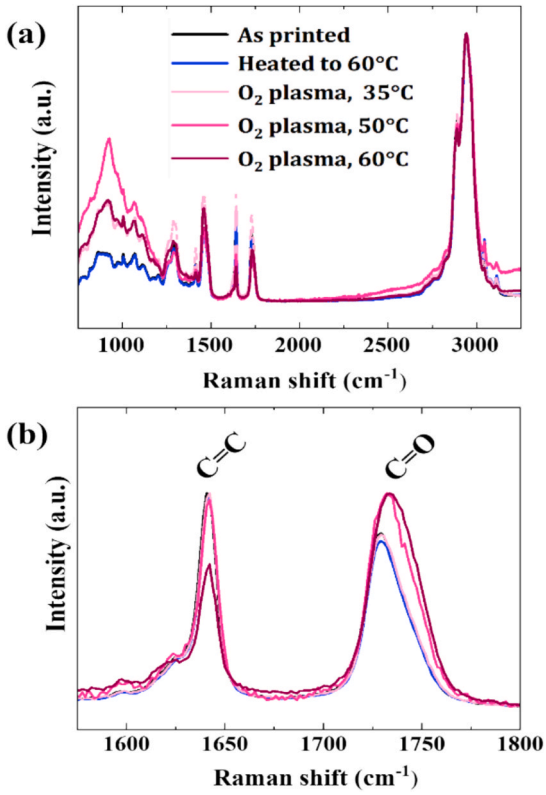

Fig. 6. Raman spectra acquired on samples treated with O_2 plasma at controlled temperature conditions. (a) Raman spectra acquired for an as printed microstructures as well as various printed samples subjected to different treatments: temperature only (20 min, 60 °C), and 20 min of O_2 plasma etching at 35°, 50 °C and 60 °C. (b) Zoom on the region displaying the peaks corresponding to the C=C and C=O bonds for all the spectra of (a), normalized in such zone for better clarity.

(1550–1800 cm^{-1}), as displayed in Fig. 6b. A remarkable change in the integrated intensities ratio of the latter peaks is already observed with the naked eye for the two samples subjected to plasma and to the highest temperatures, *i.e.* 50 and 60 °C. In fact, the normalized intensity of the C=C band of the most exposed sample (plasma and 60 °C) even becomes lower than that of its C=O band, unlike what is observed for the rest of samples.

For the estimation of the DoC, a band profile analysis was firstly performed on the Raman spectra of Fig. 6b. The obtained integrated intensities of the C=C and C=O bands were applied to Equation 1, together with those corresponding to the Raman spectrum of the reference monomer (Fig. S4). Notice that as part of a more extensive analysis of the C=C and C=O bands, we propose a simpler method for calculating the degree of crosslinking (DoC) than the one commonly used by most researchers, based on the sole analysis of the C=O band's position and width (see Supporting Information 6).

Calculated DoC values (Table 1) confirm that, while the O_2 plasma treatment at 35 °C results in no changes in the polymer to monomer

Table 1
Degree of consumption estimated from the profile analysis performed on the Raman spectra corresponding to an as printed sample and different temperature and/or plasma treated samples.

Type of sample	Temperature during treatment	DoC (%)
As printed, not treated	–	50 % ± 8
Printed, plasma-treated	35 °C	50 % ± 8
Printed, plasma-treated	50 °C	63 % ± 8
Printed, plasma-treated	60 °C	75 % ± 5
Printed, heated on hot-plate	60 °C	46 % ± 9

ratio, plasma exposure at higher temperatures yields an overall increase in the DoC: from 50 % to 63 % and 75 % for the 50 °C and 60 °C treatments, respectively. Moreover, the fact that the sample subjected to 60 °C on hot-plate (and not exposed to plasma) also presents no considerable change in DoC, indicates that, as previously reported, [22] temperature alone does not yield compositional changes before the monomer evaporation temperature is reached. All in all, these Raman outcomes suggest that the induced compositional changes are more significant when plasma and temperature effects are combined, and that such changes correspond indeed to a greater polymerization (or polymer to monomer ratio). This is in good agreement with the previously observed surface hardening as a function of O_2 plasma exposure duration, considering the simultaneously induced sample heating, which becomes more severe at longer treatment times.

3.4. Surface wettability

Control over the wettability of 3D printed microstructures is crucial in determining their interaction with their environment, as it can compromise their functionality [17,18,20,50].

O_2 plasma exposure introduces polar hydroxyl –OH groups on the surface of printed acrylate polymers, making the surface more hydrophilic and reducing the water contact angle (WCA). To complete the study, the impact of increasing exposure times on WCA has been studied, showing a rapid decrease, from a slightly hydrophilic behavior of PETA, changing from 67° to 10° in only two minutes of exposure. The results are shown in Supporting Information 7.

4. Conclusion

Post-processing strategies constitute one of the simplest ways to beat the limitations of commercially available 3D laser writing systems that rely on two-photon polymerization. Amongst the possibilities to achieve smaller printed features, etching through O_2 plasma exposure yields an isotropic thinning of the structure, with less effects on the as-cast structure physical and chemical features as compared to pyrolysis. In this work, changes in the surface properties and chemical composition have been assessed. Nanomechanical characterization of the structures exposed to O_2 plasma shows a remarkable stiffening effect on microstructure surfaces along with an increase in the surface.

roughness. Raman spectroscopy displays no surface carbonization fingerprints and no significant changes in the Degree of Consumption. These results are interpreted as very local changes occurring at the material surface in the DoC, which promote further crosslinking and selective etching of the non-reacted monomer that causes mechanical stiffening.

This effect can be further extended to the sample volume when local temperature increases, even below the monomer evaporation temperature. Raman spectroscopy results show that reactive O_2 plasma can lead to local heating capable of resulting in higher degrees of consumption. Other relevant effects such as changes in wettability have additionally been evaluated and have to be considered when plasma exposure is chosen as a post-processing method. These effects have been schematically summarized in Section 8 of Supporting Information.

Overall, this study sheds light on the physical and chemical modifications produced by O_2 plasma exposure on 3D polymeric microstructures, which despite being the simplest way to refine the feature size, the small variations induced need to be evaluated depending on the pursued application.

CRediT authorship contribution statement

Jone M. Elorrieta: Writing – review & editing, Validation, Methodology, Funding acquisition. **George Mathew:** Methodology, Investigation. **Clara Garcia-Sacristan:** Methodology, Investigation. **Jorge A.L. Solaiman:** . **Livia Martegiani:** Methodology, Investigation. **Ricardo García:** Supervision, Resources. **Eider Berganza:** Writing – original draft, Supervision, Investigation, Funding acquisition, Conceptualization.

Declaration of competing interest

The authors declare that they have no known competing financial interests or personal relationships that could have appeared to influence the work reported in this paper.

Acknowledgments

This work has been partially supported by PTA-2021-020406-I, funded by MCIN/AEI/10.13039/501100011033 and by FSE + . E.B. and G.M. acknowledge support from the Young Investigator Group Preparation Program (YIG-Prep Pro) granted by the Karlsruhe Institute of Technology. E.B. acknowledges support from the Spanish Ministry of Science in the form of a Ramón y Cajal fellowship RYC2022-036514-I. The authors acknowledge Dr. Ivan Sánchez Garcia for fruitful discussion.

Appendix A. Supplementary data

Supplementary data to this article can be found online at https://doi.org/10.1016/j.matdes.2025.115357.

Data availability

Data will be made available on request.

References

[1] H. Wang, W. Zhang, D. Ladika, H. Yu, D. Gailevičius, H. Wang, C.F. Pan, P.N. S. Nair, Y. Ke, T. Mori, J.Y.E. Chan, Q. Ruan, M. Farsari, M. Malinauskas, S. Juodkazis, M. Gu, J.K.W. Yang, Two-Photon Polymerization Lithography for Optics and Photonics: Fundamentals, Materials, Technologies, and applications, Adv. Funct. Mater. 33 (2023), https://doi.org/10.1002/adfm.202214211.
[2] W. Wang, Z.Q. Chen, B. Lin, M.C. Liu, Y. Zhang, S.J. Liu, Y. Li, Q. Zhao, Two-photon polymerization-based 3D micro-scaffolds toward biomedical devices, Chem. Eng. J. 493 (2024), https://doi.org/10.1016/j.cej.2024.152469.
[3] A. Melnikov, S. Köble, S. Schweiger, Y.K. Chiang, S. Marburg, D.A. Powell, Microacoustic Metagratings at Ultra-High Frequencies Fabricated by Two-Photon Lithography, Adv. Sci. 9 (2022), https://doi.org/10.1002/advs.202200990.
[4] F. Rajabasadi, L. Schwarz, M. Medina-Sánchez, O.G. Schmidt, 3D and 4D lithography of untethered microrobots, Prog. Mater Sci. 120 (2021), https://doi.org/10.1016/j.pmatsci.2021.100808.
[5] I. Sakellari, E. Kabouraki, D. Gray, V. Purlys, C. Fotakis, A. Pikulin, N. Bityurin, M. Vamvakaki, M. Farsari, Diffusion-assisted high-resolution direct femtosecond laser writing, ACS Nano 6 (2012) 2302–2311, https://doi.org/10.1021/nn204454c.
[6] H.B. Sun, M. Maeda, K. Takada, J.W.M. Chon, M. Gu, S. Kawata, Experimental investigation of single voxels for laser nanofabrication via two-photon photopolymerization, Appl. Phys. Lett. 83 (2003) 819–821, https://doi.org/10.1063/1.1598293.
[7] Y. Bougdid, Z. Sekkat, Voxels Optimization in 3D Laser Nanoprinting, Sci. Rep. 10 (2020), https://doi.org/10.1038/s41598-020-67184-2.
[8] F. Jin, J. Liu, Y.Y. Zhao, X.Z. Dong, M.L. Zheng, X.M. Duan, λ/30 inorganic features achieved by multi-photon 3D lithography, Nat. Commun. 13 (2022), https://doi.org/10.1038/s41467-022-29036-7.
[9] J. Fischer, M. Wegener, Three-dimensional optical laser lithography beyond the diffraction limit, Laser Photon Rev 7 (2013) 22–44, https://doi.org/10.1002/lpor.201100046.
[10] J. Fischer, M. Wegener, Three-dimensional direct laser writing inspired by stimulated-emission-depletion microscopy, Opt. Mater. Express 1 (2011) 614, https://doi.org/10.1364/OA_License_v1#VOR.
[11] C. Cao, Y. Qiu, L. Guan, Z. Wei, Z. Yang, L. Zhan, D. Zhu, C. Ding, X. Shen, X. Xia, C. Kuang, X. Liu, Dip-In Photoresist for Photoinhibited Two-Photon Lithography to Realize High-Precision Direct Laser writing on Wafer, ACS Appl. Mater. Interfaces 14 (2022) 31332–31342, https://doi.org/10.1021/acsami.2c08063.
[12] J. Askey, M.O. Hunt, L. Payne, A. van den Berg, I. Pitsios, A. Hejazi, W. Langbein, S. Ladak, Direct visualization of domain wall pinning in sub-100 nm 3D magnetic nanowires with cross-sectional curvature, Nanoscale (2024), https://doi.org/10.1039/d4nr02020k.
[13] W.E. Lu, X.Z. Dong, W.Q. Chen, Z.S. Zhao, X.M. Duan, Novel photoinitiator with a radical quenching moiety for confining radical diffusion in two-photon induced photopolymerization, J. Mater. Chem. 21 (2011) 5650–5659, https://doi.org/10.1039/c0jm04025h.

[14] V. Hahn, T. Messer, N.M. Bojanowski, E.R. Curticean, I. Wacker, R.R. Schröder, E. Blasco, M. Wegener, Two-step absorption instead of two-photon absorption in 3D nanoprinting, Nat. Photonics 15 (2021) 932–938, https://doi.org/10.1038/s41566-021-00906-8.
[15] L. Guan, C. Cao, X. Liu, Q. Liu, Y. Qiu, X. Wang, Z. Yang, H. Lai, Q. Sun, C. Ding, D. Zhu, C. Kuang, X. Liu, Light and matter co-confined multi-photon lithography, Nat. Commun. 15 (2024), https://doi.org/10.1038/s41467-024-46743-5.
[16] G. Seniutinas, A. Weber, C. Padeste, I. Sakellari, M. Farsari, C. David, Beyond 100 nm resolution in 3D laser lithography — Post processing solutions, Microelectron. Eng. 191 (2018) 25–31, https://doi.org/10.1016/j.mee.2018.01.018.
[17] J. Zhang, H. Ding, X. Liu, H. Gu, M. Wei, X. Li, S. Liu, S. Li, X. Du, Z. Gu, Facile Surface Functionalization Strategy for Two-Photon Lithography Microstructures, Small 17 (2021) 2101048–2101049, https://doi.org/10.1002/smll.202101048.
[18] X. Wang, C. Hu, L. Schurz, C. De Marco, X. Chen, S. Pané, B.J. Nelson, Surface-Chemistry-Mediated Control of Individual magnetic Helical Microswimmers in a Swarm, ACS Nano 12 (2018) 6210–6217, https://doi.org/10.1021/acsnano.8b02907.
[19] M.M. Zieger, P. Müller, E. Blasco, C. Petit, V. Hahn, L. Michalek, H. Mutlu, M. Wegener, C. Barner-Kowollik, A Subtractive Photoresist Platform for Micro- and Macroscopic 3D Printed Structures, Adv. Funct. Mater. 28 (2018), https://doi.org/10.1002/adfm.201801405.
[20] G. Mathew, E.D. Lemma, D. Fontana, C. Zhong, A. Rainer, S. Sekula-Neuner, J. Aghassi-Hagmann, M. Hirtz, E. Berganza, Site-Selective Biofunctionalization of 3D Microstructures Via Direct Ink writing, Small (2024), https://doi.org/10.1002/smll.202404429.
[21] B. Cardenas-Benitez, C. Eschenbaum, D. Mager, J.G. Korvink, M.J. Madou, U. Lemmer, I. De Leon, S.O. Martinez-Chapa, Pyrolysis-induced shrinking of three-dimensional structures fabricated by two-photon polymerization: experiment and theoretical model, Microsyst. Nanoeng. 5 (2019), https://doi.org/10.1038/s41378-019-0079-9.
[22] A. Mao, H. Mitsuboshi, M. Trochon, X. Zhang, L. Trinh, S. Keynia, P. Fan, N. Kraiem, X. Huang, N. Li, P. Li, Z. Wu, W. Sun, B. Cui, J.F. Silvain, M. Hara, M. Yoshimura, K.L. Marshall, M. Anthamatten, Y. Lu, Evolution of chemical and mechanical properties in two-photon polymerized materials during pyrolysis, Carbon N Y 208 (2023) 384–389, https://doi.org/10.1016/j.carbon.2023.03.061.
[23] P. Serles, M. Haché, J. Tam, A. Maguire, T. Li, G. Wang, K. Sebastian, J. Lou, C. Jia, P.M. Ajayan, J. Howe, Y. Zou, T. Filleter, Mechanically robust pyrolyzed carbon produced by two photon polymerization, Carbon N Y 201 (2023) 161–169, https://doi.org/10.1016/j.carbon.2022.09.016.
[24] M.I. Sharipova, T.G. Baluyan, K.A. Abrashitova, G.E. Kulagin, A.K. Petrov, A. S. Chizhov, T.B. Shatalova, D. Chubich, D.A. Kolymagin, A.G. Vitukhnovsky, V. O. Bessonov, A.A. Fedyanin, Effect of pyrolysis on microstructures made of various photoresists by two-photon polymerization: comparative study, Opt. Mater. Express 11 (2021) 371, https://doi.org/10.1364/ome.416457.
[25] W. Zhang, H. Wang, H. Wang, S. Tung Ha, L. Chen, X. Liang Li, C.-F. Pan, B. Wu, M. Abdur Rahman, Y. Ke, Q. Ruan, X. Yang, T. Christensen, J.K. W Yang, Nanoscale 3D printing of glass photonic crystals with near-unity reflectance in the visible spectrum, 2025. https://www.science.org.
[26] M. Power, A. Barbot, F. Seichepine, G.Z. Yang, Bistable, Pneumatically Actuated Microgripper Fabricated using Two-Photon Polymerization and Oxygen Plasma Etching, Adv. Intell. Syst. 5 (2023), https://doi.org/10.1002/aisy.202200121.
[27] A.J. Gross, K. Bertoldi, Additive Manufacturing of Nanostructures that are Delicate, complex, and smaller than ever, Small 15 (2019), https://doi.org/10.1002/smll.201902370.
[28] B.J. Jung, H.J. Kong, Y.H. Cho, C.H. Park, M.K. Kim, B.G. Jeon, D.Y. Yang, K.S. Lee, Fabrication of 15 nm curvature radius polymer tip probe on an optical fiber via two-photon polymerization and O2-plasma ashing, Curr. Appl Phys. 13 (2013) 2064–2069, https://doi.org/10.1016/j.cap.2013.09.011.
[29] M. Hunt, M. Taverne, J. Askey, A. May, A. Van Den Berg, Y.L.D. Ho, J. Rarity, S. Ladak, Harnessing multi-photon absorption to produce three-dimensional magnetic structures at the nanoscale, Materials 13 (2020), https://doi.org/10.3390/ma13030761.
[30] G. Williams, M. Hunt, B. Boehm, A. May, M. Taverne, D. Ho, S. Giblin, D. Read, J. Rarity, R. Allenspach, S. Ladak, Two-photon lithography for 3D magnetic nanostructure fabrication, Nano Res. 11 (2018) 845–854, https://doi.org/10.1007/s12274-017-1694-0.
[31] L.R. Meza, S. Das, J.R. Greer, Strong, lightweight, and recoverable three-dimensional ceramic nanolattices, Science 345 (2014) (1979) 1322–1326, https://doi.org/10.1126/science.1255908.
[32] S. Benaglia, V.G. Gisbert, A.P. Perrino, C.A. Amo, R. Garcia, Fast and high-resolution mapping of elastic properties of biomolecules and polymers with bimodal AFM, Nat. Protoc. 13 (2018) 2890–2907, https://doi.org/10.1038/s41596-018-0070-1.
[33] E.D. Lemma, B. Spagnolo, M. De Vittorio, F. Pisanello, Studying Cell Mechanobiology in 3D: the Two-Photon Lithography Approach, Trends Biotechnol. 37 (2019) 358–372, https://doi.org/10.1016/j.tibtech.2018.09.008.
[34] M. Taale, B. Schamberger, F. Taheri, Y. Antonelli, A. Leal-Egaña, C. Selhuber-Unkel, In Situ Fabrication of Constraints for Multicellular Micro-Spheroids using Two-Photon Lithography, Adv. Funct. Mater. 34 (2024), https://doi.org/10.1002/adfm.202302356.
[35] S.R. Dabbagh, M.R. Sarabi, M.T. Birtek, S. Seyfi, M. Sitti, S. Tasoglu, 3D-printed microrobots from design to translation, Nat. Commun. 13 (2022), https://doi.org/10.1038/s41467-022-33409-3.
[36] J. Li, P. Fejes, D. Lorenser, B.C. Quirk, P.B. Noble, R.W. Kirk, A. Orth, F.M. Wood, B.C. Gibson, D.D. Sampson, R.A. McLaughlin, Two-photon polymerisation 3D printed freeform micro-optics for optical coherence tomography fibre probes, Sci. Rep. 8 (2018), https://doi.org/10.1038/s41598-018-32407-0.
[37] R. Garcia, R. Proksch, Nanomechanical mapping of soft matter by bimodal force microscopy, in, Eur. Polym. J. (2013) 1897–1906, https://doi.org/10.1016/j.eurpolymj.2013.03.037.
[38] V.G. Gisbert, R. Garcia, Accurate Wide-Modulus-Range Nanomechanical Mapping of Ultrathin Interfaces with Bimodal Atomic Force Microscopy, ACS Nano 15 (2021) 20574–20581, https://doi.org/10.1021/acsnano.1c09178.
[39] M. Belqat, X. Wu, L.P.C. Gomez, J.P. Malval, S. Dominici, B. Leuschel, A. Spangenberg, K. Mougin, Tuning nanomechanical properties of microstructures made by 3D direct laser writing, Addit. Manuf. 47 (2021), https://doi.org/10.1016/j.addma.2021.102232.
[40] J. Lee, S.J. Park, S.C. Han, P. Prabhakaran, C.W. Ha, Enhanced mechanical property through high-yield fabrication process with double laser scanning method in two-photon lithography, Mater. Des. 235 (2023), https://doi.org/10.1016/j.matdes.2023.112389.
[41] C.S. Shin, T.J. Li, C.L. Lin, Alleviating distortion and improving the young's modulus in two-photon polymerization fabrications, Micromachines (basel) 9 (2018), https://doi.org/10.3390/mi9120615.
[42] T. Baldacchini, M. Zimmerley, C.H. Kuo, E.O. Potma, R. Zadoyan, Characterization of microstructures fabricated by two-photon polymerization using coherent anti-stokes raman scattering microscopy, J. Phys. Chem. B 113 (2009) 12663–12668, https://doi.org/10.1021/jp9058998.
[43] Z. jian Chen, J. Yao, Q. ji Xu, Z. hua Wang, Two-photon polymerization fabrication and Raman spectroscopy research of SU-8 photoresist using the femtosecond laser, Optoelectron Lett 13 (2017) 210–213. doi:10.1007/s11801-017-7043-4.
[44] L.J. Jiang, Y.S. Zhou, W. Xiong, Y. Gao, X. Huang, L. Jiang, T. Baldacchini, J.-F. Silvain, Y.F. Lu, Two-photon polymerization: investigation of chemical and mechanical properties of resins using Raman microspectroscopy, Opt. Lett. 39 (2014) 3034, https://doi.org/10.1364/ol.39.003034.
[45] S. Schweiger, T. Schulze, S. Schlipf, P. Reinig, H. Schenk, Characterization of two-photon-polymerization lithography structures via Raman spectroscopy and nanoindentation, Journal of Optical Microsystems 2 (2022) 1–12, https://doi.org/10.1117/1.
[46] Q. Hu, G.A. Rance, G.F. Trindade, D. Pervan, L. Jiang, A. Foerster, L. Turyanska, C. Tuck, D.J. Irvine, R. Hague, R.D. Wildman, The influence of printing parameters on multi-material two-photon polymerisation based micro additive manufacturing, Addit. Manuf. 51 (2022), https://doi.org/10.1016/j.addma.2021.102575.
[47] M. Diamantopoulou, N. Karathanasopoulos, D. Mohr, Stress-strain response of polymers made through two-photon lithography: Micro-scale experiments and neural network modeling, Addit. Manuf. 47 (2021), https://doi.org/10.1016/j.addma.2021.102266.
[48] Q. Hu, G.A. Rance, G.F. Trindade, D. Pervan, L. Jiang, A. Foerster, L. Turyanska, C. Tuck, D.J. Irvine, R. Hague, R.D. Wildman, The influence of printing parameters on multi-material two-photon polymerisation based micro additive manufacturing, Addit. Manuf. 51 (2022) 102575, https://doi.org/10.1016/j.addma.2021.102575.
[49] I. Henning, A.W. Woodward, G.A. Rance, B.T. Paul, R.D. Wildman, D.J. Irvine, J. C. Moore, A Click Chemistry Strategy for the Synthesis of Efficient Photoinitiators for Two-Photon Polymerization, Adv. Funct. Mater. 30 (2020), https://doi.org/10.1002/adfm.202006108.
[50] F. Tuinstra, KOENIG JL, RAMAN SPECTRUM OF GRAPHITE, J. Chem. Phys. 53 (1970) 1126–1130, https://doi.org/10.1063/1.1674108.